Open Boundary Control Problem for Navier-Stokes Equations Including a Free Surface: Data assimilation

I.Yu. Gejadze [a,*] G.J.M. Copeland [a] I.M. Navon [b]

[a]*Department of Civil Engineering, University of Strathclyde, John Anderson Building 107 Rottenrow, Glasgow, G4 0NG, UK*

[b]*Department of Mathematics, and School of Computational Science and Information Technology, The Florida State University, Tallahassee, Florida*

Abstract

This paper develops the data assimilation procedure in order to allow for the assimilation of measurements of currents and free surface elevations into an unsteady flow solution governed by the free-surface barotropic Navier-Stokes equations. The flow is considered in a 2D vertical section in which horizontal and vertical components of velocity are represented as well as the elevation of the free surface. Since a possible application is to the construction of a coastal (limited area) circulation model, the open boundary control problem is the main scope of the paper. The assimilation algorithm is built on the limited memory quasi-Newton LBFGS method guided by the adjoint sensitivities. The analytical step search, which is based on the solution of the tangent linear model is used. We process the gradients to regularize the solution. In numerical experiments we consider different wave patterns with a purpose to specify a set of incomplete measurements, which could be sufficient for boundary control identification. As a result of these experiments we formulate some important practical conclusions.

Key words: Navier-Stokes equations, Free surface, Open boundary, Optimal control, Adjoint equations, Data assimilation, Ocean, Waves
PACS:

* Corresponding author address: Dr. I.Yu. Gejadze, LMC-IMAG BP 53, 38041 Grenoble, CEDEX 9 France; Tel: 334 76635499; fax: 334 76631263

Email addresses: `igor.gejadze@imag.fr` (I.Yu. Gejadze), `g.m.copeland@strath.ac.uk` (G.J.M. Copeland), `navon@csit.fsu.edu` (I.M. Navon).

1 Introduction

The simulation of water circulation in coastal areas requires the application of advanced computer flow models. A recent tendency is to use 3D models based on the baroclinic non-hydrostatic free surface Navier-Stokes equations (fsNSE) [1], [2], [3], rather than on the shallow water equations (SWE) or the primitive hydrostatic equations (PHE). This can be explained by the fact that in coastal areas in particular we often meet baroclinic conditions (fresh water inflows), effect of topographic steering (flow separation) and non-hydrostatic situations. It may also be required to solve the bottom boundary layer. In practice, full 3D models are mostly applied as a 'zoom' designed to resolve important local details, as long as global ocean models are still based on SWE or PHE. Thus, we almost certainly face the problem of specifying boundary conditions at the open boundary of a limited area. These conditions are generally unknown. Some information could be extracted from global models, if available. However, it could be quite approximate or even incompatible (due to possible multi-physics). In order to find or to make more accurate boundary conditions at the open boundary one can use data assimilation. The boundary conditions must be recovered by a process of adjustments until the model solution agrees with measured data at the internal points of the domain. By data we will understand the velocity measurements performed by current meters and the elevations measured by tide gauges, for example. This problem can be referred to as an optimal control problem while the unknown boundary conditions are considered as controls [4]. The process of adjustment can be systematized by calculating appropriate sensitivities to guide a gradient descent algorithm.

The need of solving open boundary problem for the incompressible fsNSE represents the main difficulty of the case. Hence, there are very few rigorous results on the existence and uniqueness of the forward problem solution. For periodic boundaries the solvability of the initial boundary problem for the viscous fsNSE was proven in [5], but it took about twenty years to prove the inviscid case [6]. For fsNSE with open boundaries we are not able to mention any reference. Probably, the closest result is obtained for PHE [7]. The situation is far better with SWE. The existence of global weak solution of the viscous 2D SWE with all nonlinear terms was proven in [8]. Concerning the solvability of the open boundary control problem for fsNSE one could find even less. Optimal control theory for Navier-Stokes equations without free surface has been the concern of numerous papers, among them [9], [10], [11], [12], and for an example application one can refer to [13]. A method for assimilating the altimetry data into the solution of NSE (without considering free surface) via external stress control is proposed in [14], [15]. Here the problem for perturbations is considered in the domain with mixed boundaries (periodic and Neumann). The method requires the altimetry data to be specified everywhere or to be dense enough. These data, of coarse, may not be available in

the reality. The existence of an optimal control is proven in the case of small perturbations and a very viscous fluid only.

This paper develops the data assimilation method based on our recent results presented in [16]. In that paper we have derived the variation in the free surface variable using the mapping into a fixed domain - the approach commonly used in the aerodynamic shape optimization [17]. Then, we define the tangent linear model (TLM) and the continuous (inconsistent) adjoint model. Although we considered a 2D vertical section and the barotropic case, the extension to the full 3D baroclinic model is straightforward. Thus, we can consider that the free-surface can be treated exactly in 2D or 3D by the method in [16]. On the other hand, the open boundary is solved only approximately even for the 2D barotropic case. However, we show the way of constructing boundary conditions (BC) for the adjoint model, such that they are consistent with the approximation of open boundaries accepted in the forward model. We acknowledge the importance of characteristics in designing BC for open boundary [18]. Thus, we express fsNSE variables via variables of hyperbolic equations for which we know the characteristics and vice versa. Particularly, we use the characteristics of the 1D SWE. This sort of coupling cannot be entirely consistent, of course. However, it works quite satisfactory under the long wave assumption which need only be made at the boundaries. We control the incoming characteristic variable at the open boundary, which represents the normal incident wave. For the baroclinic case characteristics of PHE or the multi-layer SWE can be used. The extension to the 3D case is possible in the same way.

We build the data assimilation procedure based on the limited memory quasi-Newton LBFGS minimization algorithm [19], while for the step search we use analytical approach based on the solution of the TLM. Also, we introduce a regularization method, which consists of smoothing the sensitivities (gradients) by using the steepest descent or the conjugate gradient process defined in Sobolev's space [21]. This process generates a discrete family of smooth approximations, such that its Sobolev's norm is a monotonic increasing function of the iteration number. The density of this family can be controlled by the appropriate choice of the space order. The method works very well in the presence of low frequency non-periodic trends, which are usually badly approximated in orthogonal bases (for example, the Fourier basis). The need of regularization, even for exact observations, is demonstrated and explained. We design a series of numerical experiments in which we pay special attention to the assimilation of incomplete observations in different wave systems (progressive, standing and mixed waves). We recognize that reflections result in the irreversible loss of information, thus making ill-posed the inverse (control) problems for equations describing waves. In these problems, the convergence rate depends on the information available for sensors rather than on the efficiency of the minimization procedure. We formulate simple conclusions

3

concerning the lay-out of sensors. If followed in practice, it might help reduce significantly the number of iterations required for solving the control problem. That is important in real time applications. Finally we show that we can solve the open boundary control problem using local velocity observations, which differ essentially from depth-averaged values due to local non-linear effects such as eddies developing in the vicinity of sharp changes in the bathymetry.

The rapid improvement in reliability and availability of data from coastal waters is driving the need for data assimilation methods effective in tidally dominated flows. The model presented here allows direct assimilation of unsteady water levels by the adjoint method applicable to shallow tidal flows (as well as to deep water flows). Further applications for the method are to the creation of operational coastal flow models that assimilate measurements of current flows and water levels in order to calculate a 'nowcast' of flow conditions at all locations within the model area. This in turn can be used as an initial condition for a short-term forecast.

2   Problem statement

Let us consider a 2-D free surface flow in a channel, where the x - axis is directed along the channel, and the z - axis - from the channel bed to the surface. Velocities $u = u(x, z, t)$, $w = w(x, z, t)$ are associated to x, z axes respectively (see in Fig. 1). The governing equations are as follows

$$\frac{\partial h}{\partial t} + u(x, h(x, t), t) \frac{\partial h}{\partial x} - w(x, h(x, t), t) = 0 \tag{1}$$

$$\frac{\partial u}{\partial x} + \frac{\partial w}{\partial z} = 0 \tag{2}$$

$$\frac{Du}{Dt} + \frac{\partial p}{\partial x} = \Psi \cdot u \tag{3}$$

$$\frac{Dw}{Dt} + \frac{\partial p}{\partial z} + g = \Psi \cdot w \tag{4}$$

$$\frac{D \cdot}{Dt} = \frac{\partial \cdot}{\partial t} + u \frac{\partial \cdot}{\partial x} + w \frac{\partial \cdot}{\partial z}, \quad \Psi = \frac{\partial}{\partial x} \left(\mu_h \frac{\partial \cdot}{\partial x} \right) + \frac{\partial}{\partial z} \left(\mu_v \frac{\partial \cdot}{\partial z} \right)$$

$$x \in (0, L), \ z \in (H(x), h(x, t)), \ t \in (0, T))$$

where $h(x, t)$ is the elevation function describing a free surface, $H(x)$ is the channel bed shape function, L is a position of the right boundary, $\mu_h(x, z, t)$ and $\mu_v(x, z, t)$ are effective viscosities in x and z directions respectively, g is

4

the acceleration due to gravity; $p = (p_0 - p_Z)/\rho$ is relative pressure, where p_0 is pressure, p_Z - atmospheric pressure at the sea level, $\rho = const$ is density.
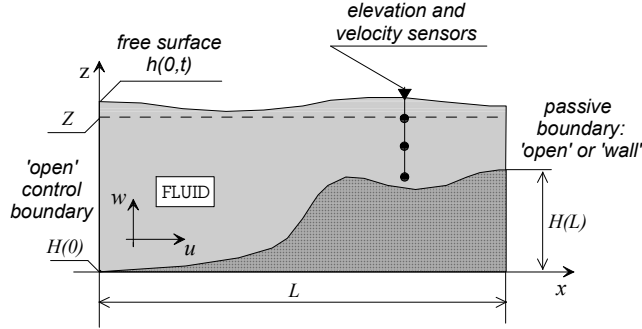

Fig. 1. Problem lay-out

The initial state is assumed to be known and we will consider it, for simplicity, as trivial

$$h(x,0) = Z, \ u(x,z,0) = 0, \ w(x,z,0) = 0 \tag{5}$$

where $Z = const$ is the elevation of the undisturbed fluid. For the channel bed $(z = H(x))$ we apply no-slip boundary conditions

$$u = 0, \ w = 0 \tag{6}$$

By neglecting the surface tension and the viscous normal stress, we have the dynamic condition for the free surface as follows

$$p = 0 \tag{7}$$

When considering boundary conditions for lateral boundaries one should distinguish between physical boundaries, where the known physical behavior of the state variables can be specified, and artificial or 'open' boundaries, introduced for computational purposes. The task of specifying boundary conditions on the open boundaries is not trivial and, in the case of systems which are predominantly hyperbolic requires a characteristic analysis of the problem to be involved. Let us assume that the open control boundary is at $x = 0$ and the passive boundary is at $x = L$. In [16] we introduce an approximate treatment of open boundaries for fsNSE using characteristic variables of SWE as follows

$$V_1 = q + (c - \bar{u})(h - Z), \ \ V_2 = q - (c + \bar{u})(h - Z) \tag{8}$$

5

where

$$\bar{u} = q/(h - H), \quad c = \sqrt{g(h - H)}, \quad q = \int\limits_{H}^{h} u \, dz \qquad (9)$$

One can note that the relationship between V_1, V_2 and primitive variables h, u of fsNSE is non-linear, unless $\bar{u}$, c and h - the upper limit of integration in the expression for q in (9) are considered as coefficients which are dependent on x, t only. The inverse relationship is also non-unique, unless we introduce an assumption concerning the distribution of u on z. Let us assume that $\bar{u}$, c and h in (9) are defined (for example, in the numerical model these values are extrapolated from the previous time step), and u is uniform through the depth. Then h, u can be linearly expressed via V_1, V_2 as follows

$$h(0, t) = Z + \frac{1}{2}\left(\frac{V_1}{c} - \frac{V_2}{c}\right)$$
$$u(0, z, t) = \frac{1}{2(h - H)}\left[\left(1 + \frac{\bar{u}}{c}\right)V_1 + \left(1 - \frac{\bar{u}}{c}\right)V_2\right] \qquad (10)$$

Now, the quantity $V_1(0, t)$, which is the incoming characteristic variable, is used as a control variable, i.e. it is as a given function, while $V_2(0, t)$ is the outgoing characteristic variable, which must be computed (using (8)) in the interior points and then extrapolated to the boundary. The boundary values for w can be calculated using the irrotationality condition that yields

$$\partial w(0, z, t)/\partial x = 0 \qquad (11)$$

For the open passive boundary at $x = L$ we write

$$h(L, t) = Z + \frac{V_1}{2c}$$
$$u(L, z, t) = \frac{1}{2(h - H)}\left(1 + \frac{\bar{u}}{c}\right)V_1 \qquad (12)$$

Now $V_1(L, t)$ is the outgoing characteristic variable, which is extrapolated from interior values. When the passive boundary represents a real physical boundary (solid/liquid interface), then the 'no-flow' conditions are considered as follows

$$h(L, t) = Z + V_1/c, \quad u(L, y, t) = 0 \qquad (13)$$

Let us denote as $\hat{h}_n := \hat{h}(x_n, t)$ elevation measurements given at some points $x_n \in (0, L)$; and as $\hat{u}_{l,m} := \hat{u}(x_l, Z_m, t)$ - u-velocity measurements at some

points $x_l \in (0, L)$ along the trajectories $Z_m := Z_m(x_l, t) \in (H(x), h(x, t))$. We formulate a boundary control problem as follows: find $V_1(t)$ and $S = [h, p, u, w]^T$ subjected to constraints (1)-(4) and boundary conditions (5)-(13) such that

$$J(V_1(t)) = inf_{(U_1)} J(U_1(t))$$

$$J(V_1(t)) = \frac{1}{2} \sum_n \int\limits_0^T (h(x_n, t) - \hat{h}_n)^2 dt$$

$$+ \frac{1}{2} \sum_l \sum_m \int\limits_0^T (u(x_l, Z_m(x_l, t)) - \hat{u}_{l,m})^2 dt \qquad (14)$$

3 Tangent linear (TLM) and adjoint model statements

The procedure for deriving the TLM and the adjoint equations in the present case is not trivial. The main difficulty consists of deriving the variation on the surface elevation function h. We use a co-ordinate transformation in the vertical to shift the problem into a domain with fixed boundaries and calculate the variation in h from the Jacobian matrix of the transformation. This variation is then mapped back into the original co-ordinate system, where the variations in the other flow parameters are calculated in a usual way. Then we use scalar product formulas re-defined for the domain with variable bounds to derive the adjoint equations and the surface and the bed boundary conditions. The detailed description of the method is presented in [16]. Thus, the TLM reads as follows

$$\int\limits_H^h 2 \left(\frac{\partial \tilde{h}}{\partial t} + u \frac{\partial \tilde{h}}{\partial x} + \frac{\partial h}{\partial x} \tilde{u} - \tilde{w} \right) \delta(z - h) dz = 0 \qquad (15)$$

$$\frac{\partial \tilde{u}}{\partial x} + \frac{\partial \tilde{w}}{\partial z} + Q_2 \cdot \tilde{h} = 0 \qquad (16)$$

$$\frac{D\tilde{u}}{Dt} + \frac{\partial \tilde{p}}{\partial x} + \frac{\partial u}{\partial x} \tilde{u} + \frac{\partial u}{\partial z} \tilde{w} + Q_3 \cdot \tilde{h} = \Psi \cdot \tilde{u} \qquad (17)$$

$$\frac{D\tilde{w}}{Dt} + \frac{\partial \tilde{p}}{\partial z} + \frac{\partial w}{\partial x} \tilde{u} + \frac{\partial w}{\partial z} \tilde{w} + Q_4 \cdot \tilde{h} = \Psi \cdot \tilde{w} \qquad (18)$$

$x \in (0, L), \ z \in (H, h), \ t \in (0, T)$.

$$Q_i \cdot \tilde{h} := a_{i,1} \frac{\partial \tilde{h}}{\partial t} + a_{i,2} \frac{\partial \tilde{h}}{\partial x} + a_{i,4}\tilde{h}, \ i = 2, 3, 4 \qquad (19)$$

7

where

$$a_{2,1} = 0, \ a_{2,2} = -\frac{z-H}{h-H}\frac{\partial u}{\partial z}, \ a_{2,4} = -\frac{1}{h-H}\left(\frac{\partial w}{\partial z} - e_2\frac{\partial u}{\partial z}\right)$$

$$a_{3,1} = -\frac{z-H}{h-H}\frac{\partial u}{\partial z}, \ a_{3,2} = -\frac{z-H}{h-H}\left(u\frac{\partial u}{\partial z} + \frac{\partial p}{\partial z}\right)$$

$$a_{3,4} = -\frac{1}{h-H}\left((w - e_1 - ue_2)\frac{\partial u}{\partial z} - e_2\frac{\partial p}{\partial z}\right)$$

$$a_{4,1} = -\frac{z-H}{h-H}\frac{\partial w}{\partial z}, \ a_{4,2} = -\frac{z-H}{h-H}u\frac{\partial w}{\partial z}$$

$$a_{4,4} = -\frac{1}{h-H}\left((w - e_1 - ue_2)\frac{\partial w}{\partial z} + \frac{\partial p}{\partial z}\right)$$

$$e_1 = \frac{z-H}{h-H}\frac{\partial h}{\partial t}, \ \ e_2 = \frac{\partial H}{\partial x} + \frac{z-H}{h-H}\frac{\partial h - H}{\partial x}$$

The initial and boundary conditions for TLM are as follows

$$\tilde{h}(x, 0) = 0, \ \tilde{u}(x, z, 0) = 0, \ \tilde{w}(x, z, 0) = 0$$

$$z = H: \ \ \tilde{u} = 0, \ \ \tilde{w} = 0$$

$$z = h: \ \ \tilde{p} = 0$$

$$x = 0: \ \ \tilde{V}_1(t) - control \ \ variable;$$

$$x = L: \ \ open \ boundary \ \ or \ \ no - flow.$$

Boundary conditions for lateral boundaries expressed via characteristic variables are given by (10)-(13) written in terms of variations in all state variables involved.

The adjoint model related to the TLM given above reads as follows

$$-\frac{\partial h^*}{\partial t} - \frac{\partial u(x, h, t)h^*}{\partial x} - \frac{\partial h}{\partial x}\frac{\partial u(x, h, t)}{\partial z}h^* - F = r_h \quad (20)$$

$$x \in (0, L), \ t \in (0, T)$$

$$-\frac{\partial u^*}{\partial x} - \frac{\partial w^*}{\partial z} = 0 \quad (21)$$

$$-\frac{Du^*}{Dt} - \frac{\partial p^*}{\partial x} - \frac{\partial w}{\partial z}u^* + \frac{\partial w}{\partial x}w^* + 2\frac{\partial h}{\partial x}h^*\delta(z - h) = \Psi \cdot u^* + r_u \quad (22)$$

8

$$-\frac{Dw^*}{Dt} - \frac{\partial p^*}{\partial z} - \frac{\partial u}{\partial x}w^* + \frac{\partial u}{\partial z}u^* - 2h^*\delta(z - h) = \Psi \cdot w^* \tag{23}$$

$$x \in (0, L), \ z \in (H, h), \ t \in (0, T)$$

where

$$F = \sum_{i=2}^{4} \left(\frac{\partial}{\partial t} \int_H^h a_{i,1} s_i^* dz + \frac{\partial}{\partial x} \int_H^h a_{i,2} s_i^* dz - \int_H^h a_{i,4} s_i^* dz \right), \tag{24}$$

$$s_i^* \in S^* = [h^*, p^*, u^*, w^*]$$

$$r_h = -\sum_n (h - \hat{h}_n)\delta(x - x_n)$$

$$- \sum_l \sum_m \left[(u - \hat{u}_{l,m})\frac{\partial u}{\partial z} \right]_{z=Z_m} \left(\frac{\partial Z_m}{\partial h} - \frac{Z_m - H}{h - H} \right)\delta(x - x_l) \tag{25}$$

$$r_u = -\sum_l \sum_m (u - \hat{u}_{l,m})\delta(x - x_l)\delta(z - Z_m) \tag{26}$$

Initial and boundary conditions for the adjoint problem are

$$h^*(x, T) = 0, \ p^*(x, z, T) = 0, \ u^*(x, z, T) = 0, \ w^*(x, z, T) = 0$$

$$z = H : \ u^* = 0 \ w^* = 0$$

$$z = h : \ p^* = 0$$

$$x = 0 : \ h^*(0, t) = \frac{c - \bar{u}}{h - H} V_1^*, \ u^*(0, z, t) = \frac{1}{h - H} V_1^* \tag{27}$$

$$x = L \ ('open') : \ h^*(L, t) = -\frac{c + \bar{u}}{h - H} V_2^*, \ u^*(L, z, t) = \frac{1}{h - H} V_2^* \tag{28}$$

$$x = L \ (no - flow) : \ h^*(L, t) = -\frac{2c}{h - H} V_2^*, \ u^*(L, z, t) = 0 \tag{29}$$

The adjoint characteristic variables V_1^* and V_2^* are defined below

$$V_1^* = \frac{1}{2c}\left(\phi^* + (c + \bar{u})q^*\right), \ V_2^* = \frac{1}{2c}\left(-\phi^* + (c - \bar{u})q^*\right)$$

where

$$\phi^* = h^*(h - H), \ q^* = \int_H^h u^* \, dz$$

The variable V_1^* in (26) and V_2^* in (28)-(29) are outgoing characteristic variables and have to be interpolated from the interior. Finally, the sensitivity (gradient) on $V_1(0, t)$ is

$$G(t) := \frac{\partial J(V_1(0, t))}{\partial V_1(0, t)} = -(c + \bar{u})V_1^*(0, t) \tag{30}$$

4 Optimization procedure and regularization

We use the limited memory quasi-Newton LBFGS method for large scale optimization [19] to perform the minimization of (14). The iterative process can be presented in the form

$$V_1^{k+1}(t) = V_1^k(t) + \beta d^k(t) \tag{31}$$

where $d^j = D(B \cdot \nabla J^k, d^{k-1}, d^{k-2}, ...)$ is a current direction of descent evaluated based on the recent gradient ∇J^k and a limited number of directions $d^{k-1}, ..., d^{k-m}$ taken from previous iteration steps; B is an operator introduced for the regularization purpose, β is a step length. The step search algorithm is a modification of a well known routine CSRCH [20]. As an initial guess we use the analytical step calculated as follows (see [21]):

$$\beta = \tilde{J}(d^k(t), \ V_1^k(t))/J(V_1^k(t)) \tag{32}$$

where

$$\tilde{J}(d^k(t), \ V_1^k(t)) = \frac{1}{2} \sum_n \int_0^T \tilde{h}^k(x_n, t) \ (h^k(x_n, t) - \hat{h}_n)dt$$

$$+ \frac{1}{2} \sum_l \sum_m \int_0^T \tilde{u}^k(x_l, Z_m(x_l, t))(u^k(x_l, Z_m(x_l, t)) - \hat{u}_{l,m})dt \tag{33}$$

The quantities $\tilde{h}^k(x_n, t)$ and $\tilde{u}^k(x_l, Z_m(x_l, t))$ are obtained by solving the TLM (15)-(19) assuming $\tilde{V}_1(t) = d^k(t)$ and $u = u^k$, $v = v^k$, $h = h^k$. If the step satisfies the sufficient decrease condition and the curvature condition, it is taken as a required value. Otherwise, the routine searches for the step around the initial guess in its own way. We should mention that the analytical step obtained via the TLM is optimal for linear problems (because the TLM coincides with an original problem). It works well for non-linear problems if the non-linearity is moderate, i.e. it does not strongly dominate the system behavior. Otherwise,

10

we should return to the non-analytical step search methods (for example, the gold section method, as implemented in CSRCH).

Another important issue is a regularization. It is well known that most inverse problems are ill-posed in some sense. For example, the inverse operator may be unbounded. As a result, errors of different nature are amplified and assimilated into the solution. The foundations of regularization theory had been developed by A.N.Tikhonov [24] in early 1960's. For a state-of-art practical review on this subject one can refer to [25]. It is observed that the Tikhonov method is not particularly efficient if the problem is solved by iterative methods. The main reason here is that the choice of the regularization parameter is not transparent, i.e. one may proceed by trial and error approach, that could be rather expensive in terms of computational costs. Another drawback is that in the non-linear case introducing penalty terms may generate additional points of zero variation. That is why different regularization methods had been proposed [21], [23]. The basic idea of these methods consists of restricting the control space. In [23] the multi-level (wavelet) representation of control functions is used, while the decision concerning the appropriate level is taken based on the analysis of the minimal eigenvalue of the Hessian. The efficiency of this approach depends on the distribution of eigenvalues associated to the problem of interest. In fact, in case of the diffusion equation rather a few leading eigenvalues have to be considered. In [21] the control function is updated in the Sobolev's space W_2^p of order p. One can note, however, that the choice of p is not obvious either. In our case even using of W_2^1 proves redundant, because it slows the convergence rate drastically. To avoid this difficulty we use the approach as follows. Let us consider a function $f(t)$ and its generalized norm as follows

$$\|f(t)\|_{W_2^p}^2 = \int\limits_t^T \sum\limits_0^p \left(\frac{d^p f(t)}{dt^p}\right)^2 dt$$

We would like to construct a family of functions g^m which successively approximate f in a manner that $\|g^m - f\|_{W_2^0}$ is a decreasing function of m, while $\|g^m\|_{W_2^2}$ is a monotonic increasing function of m. It is suggested in [21] that such a family can be generated by an iterative process based on the steepest descent (SD) or on the conjugate gradient (CG) method working in Sobolev's spaces. For example, the SD method in W_2^1 can be presented as follows:

$$g^{m+1}(t) = g^m(t) - \beta_0 P^m(t) - \beta_1 Q^m, \quad g^0 = f(0) \tag{34}$$

$$P^m(t) = \int\limits_0^t \int\limits_\xi^T (g^m(\eta) - f(\eta)) d\eta \ d\xi, \quad Q^m = \int\limits_0^T (g^m(t) - f(t)) dt \tag{35}$$

11

At each iteration step the parameters β_0 and β_1 must be calculated to minimize the norm $\|g^{m+1}(t) - f(t)\|_{\bar{W}_2^0}$. By choosing m we can always find an approximation to f, which we believe is reasonably 'smooth' compared to f itself. For example, we can suggest the criterion as follows: increase m until

$$\frac{\|g^m(t) - f(0)\|_{W_2^2}}{\|f(t) - f(0)\|_{W_2^2}} < \alpha \frac{\|g^m(t) - f(t)\|_{W_2^0}}{\|f(0) - f(t)\|_{W_2^0}}, \quad 0 < \alpha \le 1 \tag{36}$$

Since we use the initial approximation $g^0(t) = f(0)$, at first the left-hand side of (36) is equal to zero and the right-hand side - to α. By (36) we actually demand that the convergence $g^m(t)$ to $f(t)$ in $W_2^0 \equiv L_2$ should be faster (up to the factor α) than the convergence of their W_2^2-norms. When we put $f = \nabla J^k$, the iterative process (34), (35) along with the stopping criterion (36) define the action $B \cdot \nabla J := g^{m+1}$, which is used by LBFGS. Because the control function is a weighted sum of the gradients from all iterations it must belong to the same solution space as gradients. If we treat the gradient as suggested above, the overall iterative process (31) is not biased (in contrast to the Tikhonov method). The iterations must converge to the minimum of (14). However, the process is ordered in the sense that $\|V_1^k(t)\|_{W_2^2}$ is supposed to be a monotonic increasing function of the iteration number k.

5 Numerical examples

5.1 General description of the numerics

A trial numerical implementation has been made using a finite-difference semi-explicit solution of the problem with a fixed regular mesh similar to the well known SOLA algorithm [22]. Equations are discretized on a staggered grid using a hybrid scheme for advection terms. The Poisson equation for pressure is formed and solved by the SOR method in the case of the forward equations and the TLM, and by a direct solver based on banded LU-decomposition in the case of the adjoint equation. In solving the forward model, the solution h, p, u, w is saved in the memory. This data is recalled when the TLM or the adjoint problem is running. Because the forward, the TLM and the adjoint equations differ only in source terms a single solver is used. The numerical experiments carried out here are usually referred to as 'identical twin experiments'. For a certain value of the control function $V_1(t)$ we perform the forward run. The solution at the measurement points is interpreted as observations (measured data record). Then, the control function $V_1(t)$ is considered as the unknown function that has to be estimated in the course of the data assimilation procedure, while the difference $\delta V_1(t) := V_1(t) - V_1^k(t)$ defines

the estimation error. For minimization of the objective functional (14) we use LBFGS using the analytical step search as described above. We start from the trivial initial guess $V_1^0(t) \equiv 0$ in all assimilation tests that follow. If no special stopping criterion is used, the iterative process is terminated by the step search routine, when it recognizes the direction suggested is not a direction of descent.
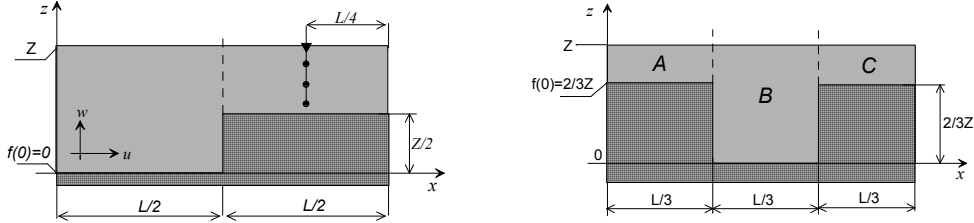

Fig. 2. Channel bathymety. **Left** - a 'step', **right** - a 'pit'.

In order to underline a general applicability of the method we design special test cases when the bed function suddenly changes from being deep to shallow (and vice versa). In reality this describes a situation near the 'shelf' edge, which is essentially non-hydrostatic. The change happens over one space discretization step, i.e. dH/dx always remains bounded. The two channel geometries called 'step' and 'pit' are shown in Fig.2(left/right). Channel dimensions are: $L = 3000\ m$, $Z = 100\ m$ for the bathymetry 'step', and $L = 5000\ m$, $Z = 200\ m$ - for the 'pit'. The number of grid nodes used in all calculations presented here is $N_x = 100$ and $N_z = 20$, and the time discretization step is $\Delta t = 0.36\ s$. All the computations are performed for viscous flow assuming $\mu_v = 0.1$, but $\mu_h = 0$.

The bathymetry is chosen to enable consideration of a few possible wave patterns. If the open right boundary is used, then we observe clean progressive waves in section B for the bathymetry 'step', and in section C for the 'pit'. Measurements within section B for the 'step' contain the same components as the boundary control function $V_1(t)$, shifted in time and scaled at the step. In this case the data assimilation problem is nearly trivial and the iterations converge very quickly (see Fig.6). The situation is more complicated while considering the bathymetry 'pit'. Here incident waves are partially reflected from the right step, then the reflected part is partially reflected from the left step and goes toward the right boundary and so on. As a result, in addition to waves directly arriving from the control boundary, measurements within section C contain secondary (tertiary, etc.) signals originated within section B. These waves enter section C along the incoming characteristics. Therefore, we still have the progressive wave here, but the assimilation algorithm has to filter the incident signal out of the mix. The assimilation example for this case is given in Fig.9(left/right).

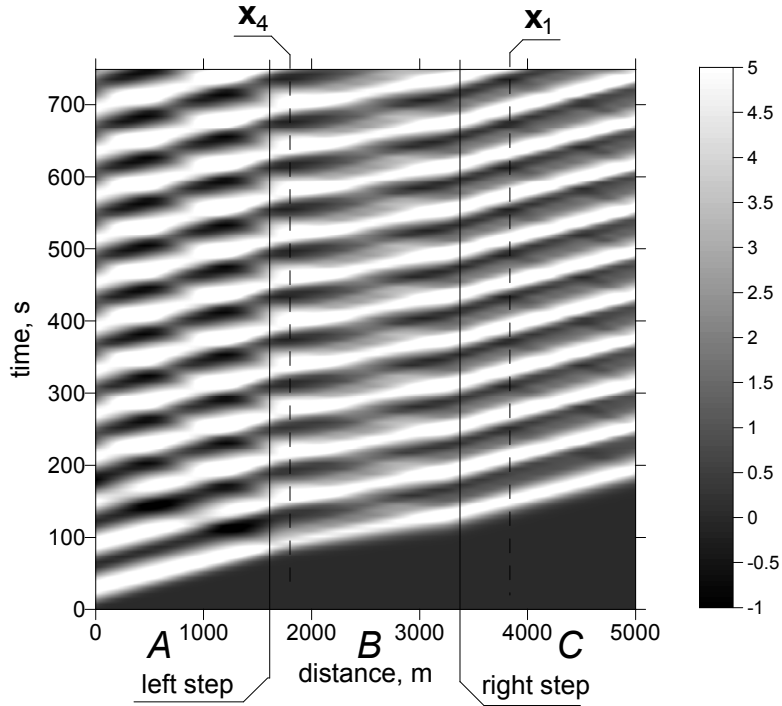In section A for the bathymetry 'step' and in sections A and B for the 'pit'

13

Fig. 3. The surface elevation: open right boundary and bathymetry 'pit' in Fig.2(left)
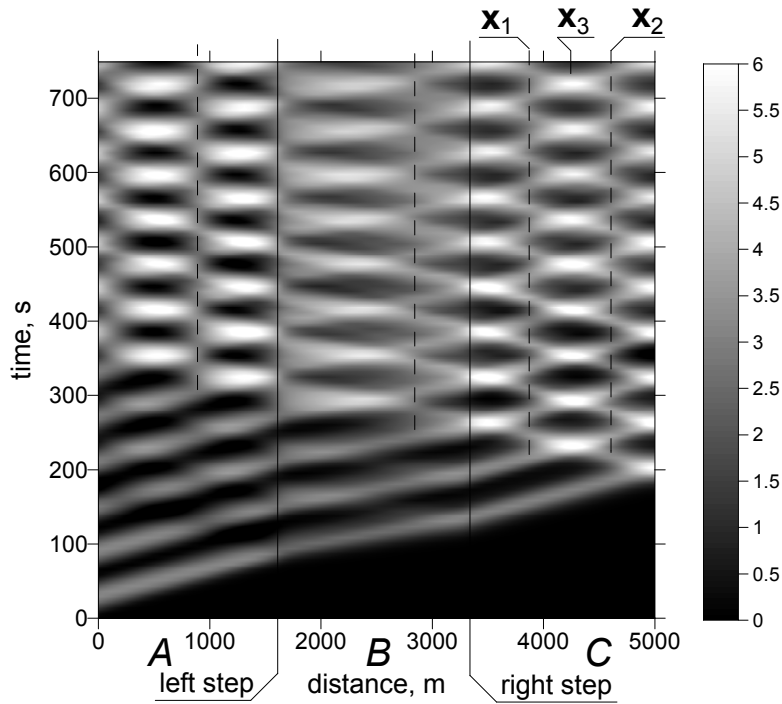

Fig. 4. The surface elevation: no-flow right boundary and bathymetry 'pit' in Fig.2(right)

we observe a combination of progressive and standing waves (it is worth to underline that reflections always occur if $|\partial H/\partial x \neq 0|$. If sensors are located in these areas, the assimilation problem becomes more complicated. The sit-

14

uation is different because information propagates in both directions, i.e. as from the control boundary to the sensors, so from the opposite side. Nevertheless, if the right boundary is open, the wave regime here is dominated by a progressive wave. The surface elevation for the bathymetry 'step' with the open right boundary can be seen in Fig.3. When the no-flow right boundary is used, we observe standing waves throughout the channel, see Fig.4. This is the least favorable case for the data assimilation via boundary control. Now the information is re-distributed over the spatial domain and some sensors may turn out to be located in the areas of the low informational content. For example, the elevation sensors could be located in the wave nodes shown by dashed lines in Fig.4, where the surface is almost motionless. Obviously, such measurements carry very little dynamic information that raises the issue of solvability.

In order to generate the control function $V_1(t)$ we use the expression as follows

$$V_1(t) = \frac{ZA}{2}\left(1 + sin\left(\frac{3\pi}{2} + \frac{\pi t}{P}\right)\right) \tag{37}$$

where $A[m/s]$ is the amplitude and $P[s]$ is the wave period. Equation (37) defines a 'lifted' sinusoid which generates simultaneously the two phenomena: a periodic wave and a rise of the mean flow level. That produces a non-zero mean flow and causes eddies to develop in the vicinity of steps. We introduce also two additional notations to describe results. The first one denotes the norm of the gradient $G^k := \|\nabla J^k(t)\|_{L_2(0,T)}$, the second one - the norm of the estimation error $Q^k := \|\delta V_1(t)\|_{L_2(0,T-\delta T)}$, where δT is the length of a 'blind' spot. This is a time interval required for a perturbation from the nearest sensor to reach the control boundary. We will consider relative values J^k/J^0, G^k/G^0 and Q^k/Q^0 presented in the logarithmic scale. The summary of numerical experiments is given in Table 1.

5.2   On a need of regularization

It is well known that inverse problems are generally ill-posed. Thus, the solution method must be robust in respect to errors. One of these errors is related to the initial 'shock' in the adjoint solution, which results from the discontinuity of the residuals r_h and r_u at $t = T$. In order to illustrate this effect we consider numerical examples using the bathymetry 'step' and the open right boundary. We assume that the velocity and the elevation sensors are located in the middle of section B, where we observe a clean progressive wave. Let us take a look at Fig.5(left). Here *line 1* shows the control function $V_1(t)$, *line 2* - the depth averaged inlet velocity $\bar{u}(0,t)$, *line 3* - the velocity data record $\hat{u}(x_1,t)$ and *line 4* - the elevation data record $\hat{h}(x_1,t)$. First we

15

choose T such that $\hat{h}(\cdot, T)$ and $\hat{u}(\cdot, T)$ are small and, therefore, the residuals $r_h(T) = h^0(\cdot, T) - \hat{h}(\cdot, T)$ and $r_u(T) = u^0(\cdot, T) - \hat{u}(\cdot, T)$ are small too. We solve the control problem assimilating these data. The results are presented in Fig.6(left). Here, the three cases referred to as 'a', 'b' and 'c' correspond to different values of the wave period P in (37): 'a' - $P = P_0$, 'b' - $P = P_0/2$, 'c' - $P = P_0/4$. Convergence history results are presented as follows: *line1* shows $\log(J^k/J^0)$, *line 2* - $\log(Q^k/Q^0)$, and *line 3* - $\log(G^k/G^0)$. As we mentioned before, the case when we can observe a clean primary progressive wave is the most favorable. Thus, the iterative process has converged to a minization threshold just in few steps. We can note, however, that the convergence depth depends on the wave-length: the shorter are waves, the larger is the minimization threshold. This effect is apparently related to the approximate treatment of open boundaries. Indeed, we construct control invariants for the barotropic fsNSE using characteristics of SWE. These two models are consistent when describing a hydrostatic flow, i.e. in the long-wave case. We should mention that the solution corresponding to the shortest wave period in case 'c' is not yet a short wave. However, the solution errors, particularly generated by the 'shock', contain high frequency components, which are short waves for the model. These components do not entirely leave the computational domain via 'approximate' open boundaries and could survive long if not dissipated by the viscous terms. In order to magnify this effect we choose the observation window shorter than in previous examples ($T \approx 690s$), as it is shown by vertical line in Fig.5(left). We note that $\hat{h}(\cdot, T)$ and $\hat{u}(\cdot, T)$ are now close to their maximum values. The initial discontinuity in source terms r_u and r_h generates oscillations in the adjoint solution, which should normally pass through the computational domain and vanish. In the case of an approximate boundary treatment these oscillations are partially reflected back creating new errors. In Fig.6(right) we can see the convergence history for $P = P_0$, which is given in *lines 1b,2b*. The corresponding result from Fig.6(left) is presented here for comparison in *lines 1a,2a*. The difference in the minimization depth achieved in these two cases is more than obvious. Let us now look at Fig.5(right). Here *line 1* shows the control function $V_1(t)$, *line 2* - the estimation error in the case without initial 'shock', *line 4* - the estimation error in the case of a strong initial 'shock'. Next, we apply regularization as described in Section 4 ($\alpha = 1$ in (36)). The convergence history is presented in *lines 1c,2c* in Fig.6(right), while the corresponding final estimation error in *line 3* in Fig.5(right). It can be seen that the latest result is essentially better: regularization allowed oscillations to be suppressed and achieve more than an order of magnitude smaller values of J and Q. On the other hand it slowed the convergence rate. (Remark. Although the regularization of that type may slow the convergence rate it can be seen only in those simple cases as above, when the process converges in few iterations. In more complicated cases we may need more iterations to solve the control problem anyway and this 'side' effect of regularization should not be noticeable).
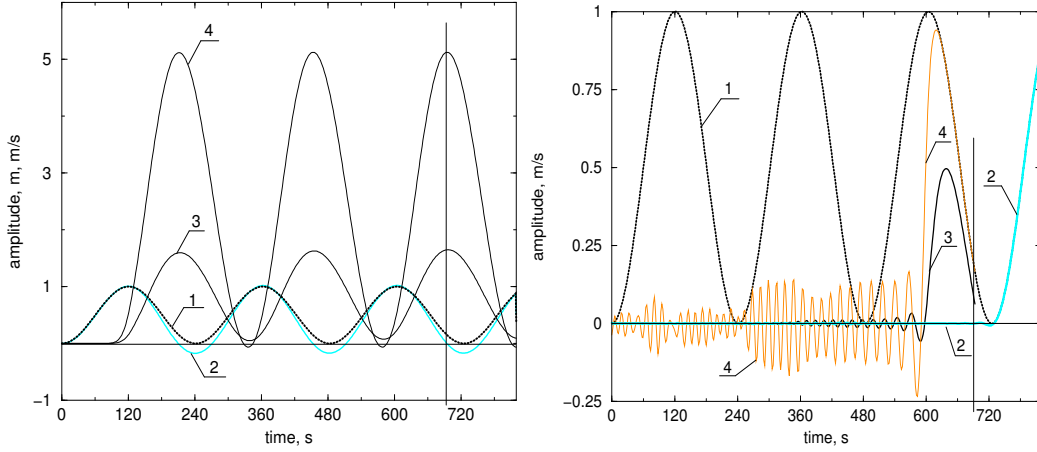
Fig. 5. **Left.** Control variable $V_1(t)$ - line 1 and solutions from the forward model: depth averaged inlet velocity $\bar{u}(0,t)$ - line 2; data records $\hat{u}(x_1, z_1, t)$ - line 3 and $\hat{h}(x_1, t)$ - line 4. **Right.** Control variable $V_1(t)$ - line 1 and control problem solution: estimation errors - lines 2,3,4.
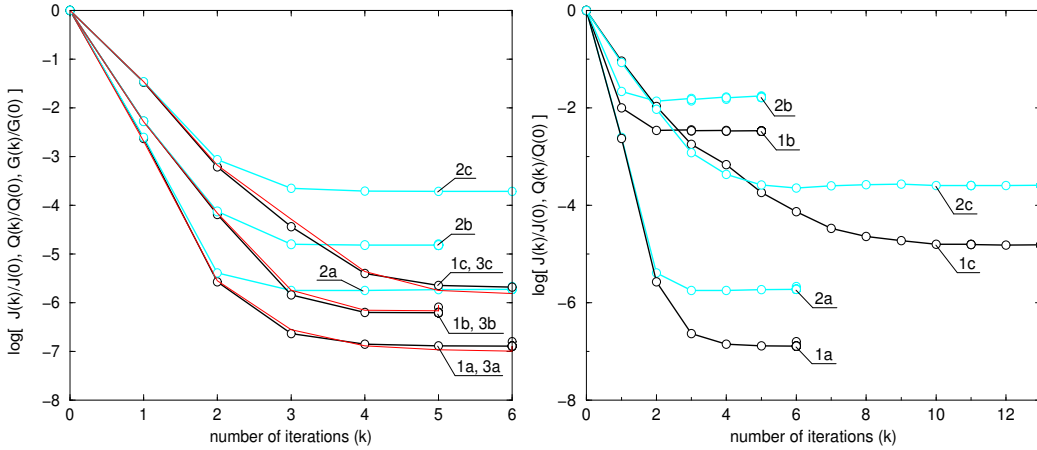

Fig. 6. **Left.** Convergence history with an insignificant initial 'shock' for different values of the wave-length. **Right.** Convergence history with a strong initial 'shock': without regularization - lines 1b, 2b; regularized solution - lines 1c, 2c.

Another source of errors is, of course, a measurement error. This is not necessarily an instrumental error. For example, in addition to long waves, which are of main concern in applications related to the oceanography, the real case could contain short waves induced by a random wind stress. If these waves cannot be presented at a certain level of discretization, they should be regarded as the measurement error, since sensors measure real physical values. The error of that type is sometimes called the 'representation' error.

In the next numerical experiment we consider the same test example as in Fig.5(left), with the observation window $T = 690s$. The records $\hat{u}(x_1, t)$ (in *line 3*) and $\hat{h}(x_1, t)$ (in *line 4*) are now contaminated by Gaussian noise with mean values $\sigma_u = 0.3ms^{-1}$ and $\sigma_h = 1m$ correspondingly. The noise is essentially comparable to the useful signal. The results of solving the control
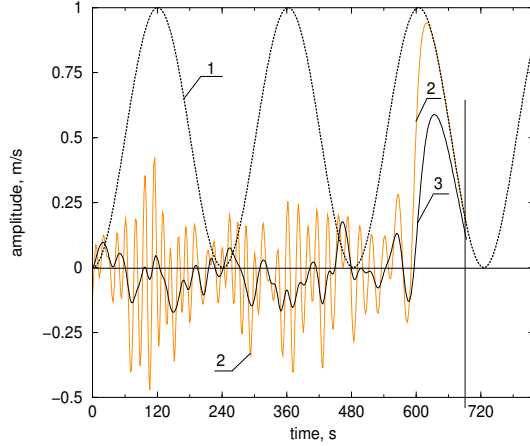
17

Fig. 7. Control variable $V_1(t)$ - line 1 and control problem solution: estimation errors in the presence of observation noise without regularization - line 2; regularized - line 3.

problem are presented in Fig.7. Here, *line 1* shows $V_1(t)$, *line 2* - the estimation error without regularization, *line 3* - the estimation error when using regularization. In the last case the iterative process has been stopped by the residual rule [26] after the third iteration. We note that the estimation error is now much smaller and the solution do not exhibit that strong oscillatory behavior. In conclusion, numerical examples show the need of regularization to build a robust data assimilation algorithm. The efficiency of the regularization method suggested in Section 4 is also demonstrated. We use regularization in all numerical examples that will follow.

5.3 On a need for co-located measurements

In Section 5.1 we described different wave patterns. Then, in Section 5.2 we considered the simplest assimilation case, where the clean primal progressive wave was observed. More complicated wave pattern arises when we chose the bathymetry 'pit'. We assume that sensors are located in section C at $x = x_1$ as shown in Fig.3. In this case observations contain both a primal signal delivered directly from the control boundary and signals resulted from reflections, which occur in the cavity in section B. However, all perturbations in section C propagate from the left to the right, i.e. belong to the only one characteristic family. To demonstrate this effect more clearly we choose the wave-length that is comparable to the size of the cavity. The results of the forward modeling are presented in Fig.8(left). Here *line 1* shows the control function $V_1(t)$, *line 2* - the depth averaged velocity $\bar{u}(0, t)$, *line 3* - the velocity record $\hat{u}(x_1, t)$, *line 4* - the elevation record $\hat{h}(x_1, t)$. The surface pattern related to this case is shown in Fig.3. Looking at the records $\hat{u}(x_1, t)$ and $\hat{u}(h_1, t)$ we note that they are apparently complex, although $V_1(t)$ contains only one harmonic component. The results of solving the control problem are presented in Fig.9(left). Here

18

line 1 shows the convergence history when both $\hat{u}$ and $\hat{h}$ are assimilated, *line 2* - when only $\hat{u}$ is assimilated, *line 3* - when only $\hat{h}$. We can see that the iterative process converges almost equally in all these cases. This example illustrates an important result on the solvability of the open boundary control problem, which can be formulated as follows: *if the sensors are located in a progressive wave area, then measurements of the elevation or the velocity profile performed at a single location provide necessary and sufficient information to identify the boundary control $V_1(t)$.*
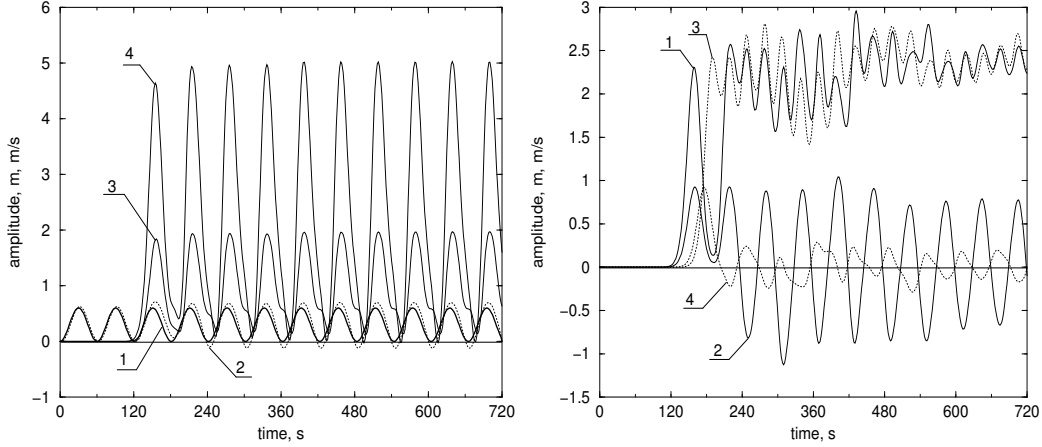

Fig. 8. Left. Control variable $V_1(t)$ - line 1 and solutions from the forward model (open right boundary): depth averaged inlet velocity $\bar{u}(0,t)$ - line 2; data records $\hat{u}(x_1, z_1, t)$ - line 3 and $\hat{h}(x_1, t)$ - line 4. **Right.** Solutions from the forward model (no-flow right boundary): data records $\hat{u}(x_1, z_1, t)$ - line 2; $\hat{h}(x_1, t)$ - line 1; $\hat{u}(x_3, z_1, t)$ - line 4; $\hat{h}(x_2, t)$ - line 3.
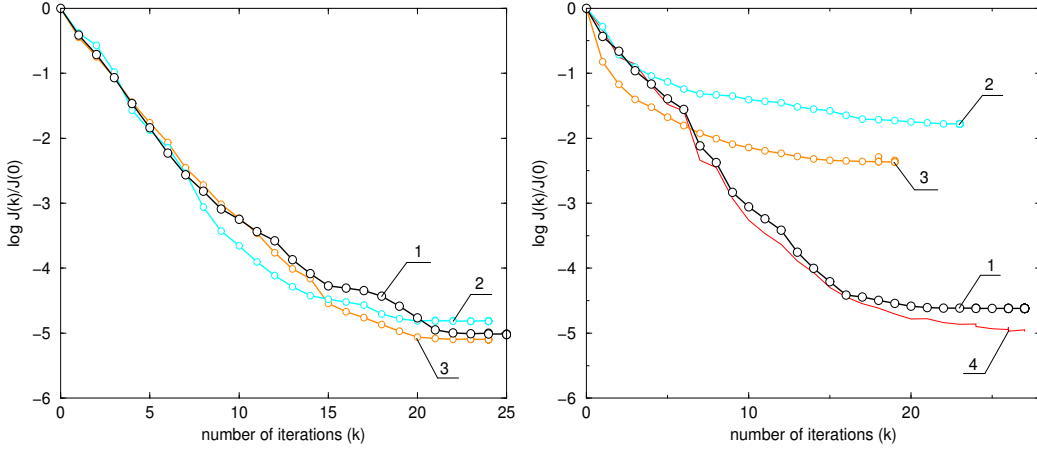

Fig. 9. Convergence history $J(k)/J(0)$. **Left** - open right boundary: both $u(x_1, y_1, t)$ and $h(x_1, t)$ are assimilated - line 1; only $u(x_1, y_1, t)$ is assimilated - line 2; only $h(x_1, t)$ is assimilated - line 3. **Right** - no-flow right boundary: both $u(x_1, y_1, t)$ and $h(x_1, t)$ are assimilated - line 1; corresponding $G(k)/G(0)$ - line 4; only $u(x_1, y_1, t)$ is assimilated - line 2; only $h(x_1, t)$ is assimilated - line 3.

Next we consider the no-flow right boundary, which produces standing waves throughout the channel. As we mentioned before, information is now redistributed over the spatial domain. Thus, the success of solving the control
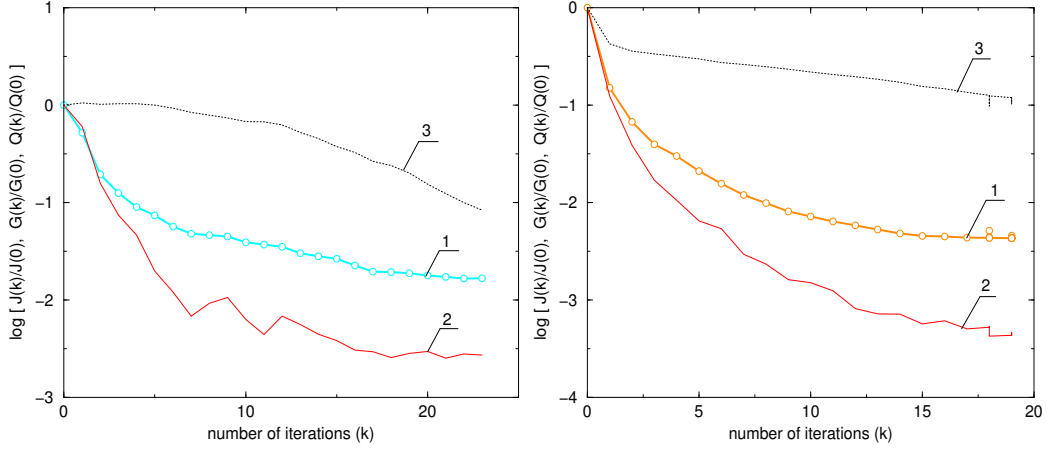
19

Fig. 10. Convergence history (no-flow right boundary). **Left:** only $u(x_1, y_1, t)$ is assimilated. **Right:** only $h(x_1, t)$ is assimilated. $J(k)/J(0)$ - line 1; $G(k)/G(0)$ - line 2; $Q(k)/Q(0)$ - line 3.
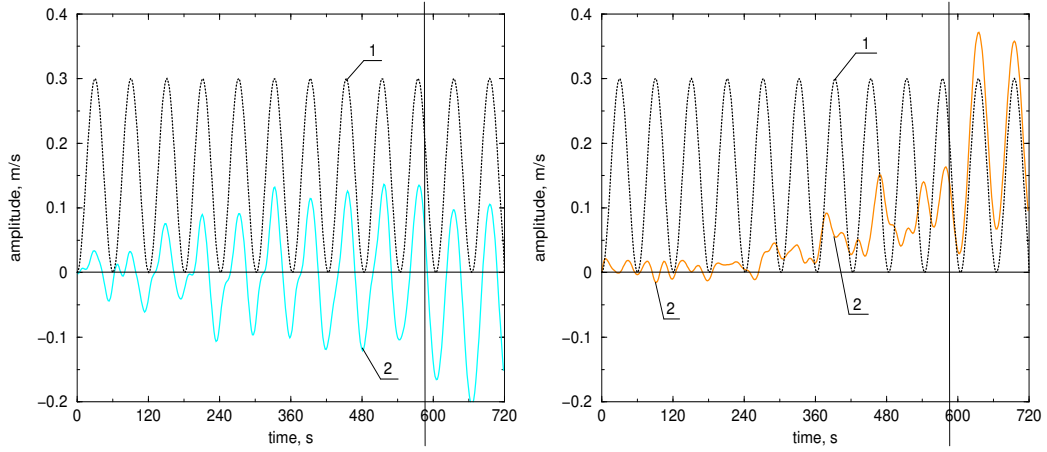

Fig. 11. Control problem solution (no-flow right boundary). Control function $V_1(t)$ - line 1; final estimation error - line 2. **Left:** only $u(x_1, y_1, t)$ is assimilated. **Right:** only $h(x_1, t)$ is assimilated.

problem may depend on the information content available for sensors. We consider several sensor configurations in order to show that only co-located measurements of the elevation and the velocity do provide sufficient information to identify the boundary control. Results of forward modeling are presented in Fig.8(right). The control function $V_1(t)$ is given by *line 1* in Fig.8(left), and the corresponding surface elevation is given in Fig.4. We also show here locations of sensors x_i. The data records are presented in Fig.8(right). Here *line 1* shows $\hat{h}(x_1)$, *line 2* - $\hat{u}(x_1)$, *line 3* - $\hat{h}(x_2)$, *line 4* - $\hat{u}(x_3)$. The results of solving the control problem are presented in Fig.9(right). Here *line 1* shows the convergence history when both $\hat{u}(x_1, t)$ and $\hat{h}(x_1, t)$ are assimilated, *line 2* - when only $\hat{u}(x_1, t)$ is assimilated, *line 3* - when only $\hat{h}(x_1, t)$. We intentionally put sensors in the surface elevation node, where the real dynamics of $V_1(t)$ cannot be directly observed neither in $\hat{h}(x_1, t)$, nor in $\hat{u}(x_1, t)$ (apart from a short time interval at the beginning). If we use both, this allows to minimize the objective functional deeply enough and obtain a good quality

solution. On the contrary, if we assimilate $\hat{u}(x_1, t)$ or $\hat{h}(x_1, t)$, the iterative process stops converging at quite a shallow minimization level. To understand the reason it is worth looking at the behavior of $G(k)/G(0)$ compared to the behavior of $J(k)/J(0)$ in Fig.9(right). In the first case ($\hat{u}$ and $\hat{h}$) the behavior of the relative gradient norm $G(k)/G(0)$ in *line 4* is nearly the same as behavior of $J(k)/J(0)$ in *line 1*. The two lines start to diverge only when approaching the minimization threshold. The same sort of behavior can be seen, for example, in Fig.6(left) under different circumstances. For the second case ($\hat{u}$ or $\hat{h}$) results are presented in Fig.10 (left/right). Here *line 1* shows $J(k)/J(0)$, *line 2* - $G(k)/G(0)$, *line 3* - $Q(k)/Q(0)$. The left part corresponds to *line 2* and the right one - to *line 3* in in Fig.9(right). This figure shows that $G(k)/G(0)$ quickly becomes much smaller than $J(k)/J(0)$, i.e. the residuals of a certain level produce incomparably smaller gradient. This apparently indicates that the information content could be assimilated very slowly or it is already exhausted. In addition we should look at the final estimation error presented in Fig.11(left/right) correspondingly. Here *line 1* shows the control function $V_1(t)$, *line 2* - the estimation error. We note that the estimation error is a function containing essentially the same as a control function frequency components or lower, i.e. it is obviously a systematic assimilation error.

In the next example we assimilate observations from the elevation and the velocity sensors, but located at two different positions: $\hat{h}(x_1, t)$ and $\hat{u}(x_3, t)$. We note that x_3 is located between the two elevation nodes x_1 and x_2. Since there is a phase shift $\pi/2$ between h and u, x_3 is the velocity wave node. The convergence history for this case is shown in Fig12, *line 2*.
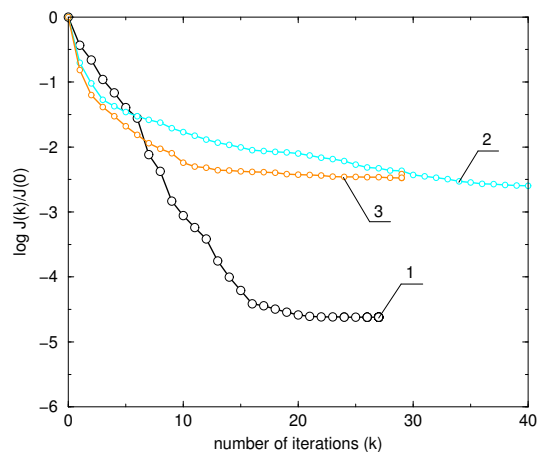

Fig. 12. Convergence history $J(k)/J(0)$ (no-flow right boundary). Both $u(x_1, y_1, t)$ and $h(x_1, t)$ are assimilated - line 1; non co-located $u(x_3, y_1, t)$ and $h(x_1, t)$ are assimilated - line 2; both $h(x_1, t)$ and $h(x_2, t)$ are assimilated - line 3.

Here *line 1* shows the same convergence history as in Fig9(right). The example shows the importance of the sensor location: the complementary velocity data has to be measured in the same point as the elevation data. In addition

we assimilate measurements from two elevation sensors located at x_1 and x_2 correspondingly. The convergence history is presented in Fig.12, *line 3*. Those examples show that the convergence is warranted only if using co-located measurements of u and h. In practice we should interpret the term 'co-located' considering the wave-length scale, of course. Thus, another result on the solvability of the open boundary control problem can be formulated as follows: *if the sensors are located in the area where standing waves occur, then co-located measurements of the elevation and the velocity profile are needed to provide necessary (but maybe not yet sufficient) information to identify the boundary control $V_1(t)$.*

5.4   On a benefit of the cross-sectional resolution

There are several reasons why we may need the cross-sectional resolution and, therefore, should use models other than SWE. In the 2D case the important reason could be that $u(x, z, t)$ is not uniform in depth ($v(x, z, t)$ can be other than the linear function of z). When using SWE, we should measure the discharge or the depth averaged velocity. In reality we may have a single velocity sensor located at a certain depth. For example, one could measure the Lagrangian data, i.e. the dynamic trajectory of a float that gives velocity estimation at the surface. The surface value may differ significantly from the depth averaged value, of course. Thus, if the measured local velocity is interpreted as a depth averaged velocity by the SWE model, then the solution of the control problem could contain an essential error. We design numerical experiments to show that when using fsNSE, the control problem can be correctly solved based on local velocity measurements. For tests we use the bathymetry 'pit' with the open right boundary. In order to generate eddies we use the longer observation window $T = 1h$, and the control function $V_1(t)$ as shown in Fig.13(left), *line 1*. Then we consider the two cases.

In the first case (referred to as 'a') we use only data from the velocity sensor located at x_1 (see Fig.3) in the grid node that is the nearest to the channel bed. The velocity data record $\hat{u}$ is given in Fig.13(left) *line 2*. For comparison, the depth averaged value of the velocity $\bar{u}$ is shown here by *line 3*. In the second case (referred to as 'b') we use the the velocity sensor located at x_4 in the grid node that is the nearest to the surface. The velocity record is given in *line 2*, Fig.13(right), and the data record of a co-located elevation sensor is given here in *line 1*. The depth averaged velocity $\bar{u}$ is shown in *line 3* for comparison. In both cases we should pay attention to the difference between the local velocity and the depth averaged velocity values. The convergence history is presented in Fig.13. Here for the two cases 'a' and 'b' as described above *line 1* shows $J(k)/J(0)$, *line 2* - $Q(k)/Q(0)$ and *line 3* - $G(k)/G(0)$. The first example shows that we were able to find the boundary control even
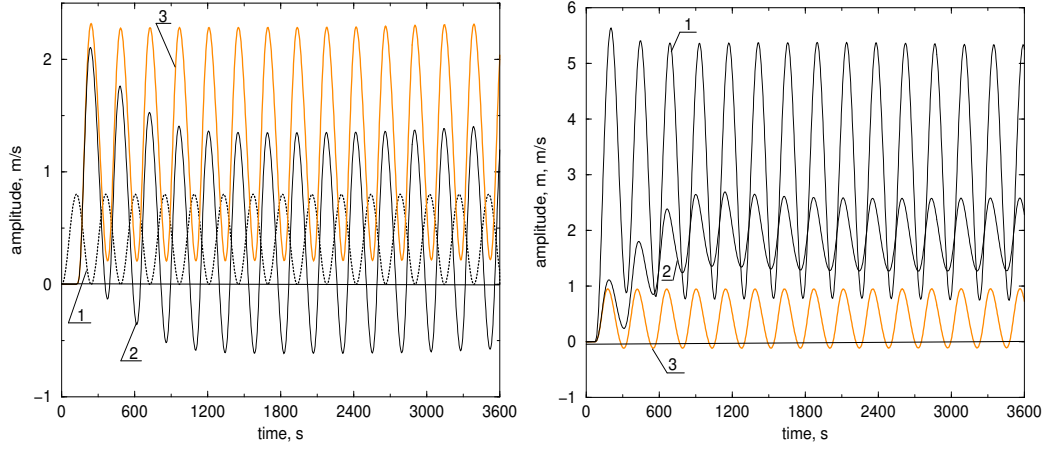
22

Fig. 13. **Left.** Control variable $V_1(t)$ - line 1 and solutions from the forward model (open right boundary): near bed velocity record $\hat{u}(x_1, z_1, t)$ - line 2; depth averaged velocity $\bar{u}(x_1, t)$ - line 3. **Right.** Solutions from the forward model (open right boundary): elevation record $\hat{h}(x_4, t)$ - line 1; near surface velocity records $\hat{u}(x_4, z_1, t)$ - line 2; depth averaged velocity $\bar{u}(x_4, t)$ - line 3.

though the sensor was located within the eddy. The process required many iterations to be completed, but had been steadily converging and converged to a deep minimization threshold. In the second case we observe much faster convergence because of using the co-located elevation data.
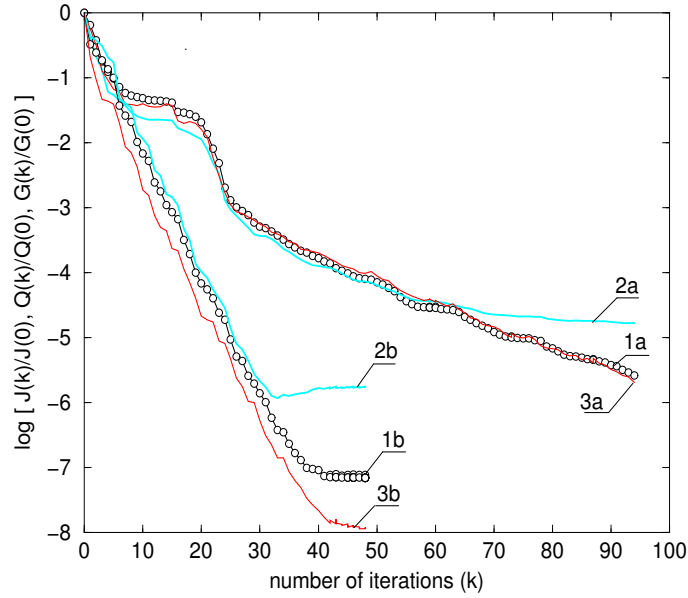

Fig. 14. Convergence history: $J(k)/J(0)$ - lines 1a/1b; $Q(k)/Q(0)$ - lines 2a/2b; $G(k)/G(0)$ - lines 3a/3b. **Case 'a'** - $\hat{u}(x_1, z_1, t)$ is assimilated. **Case 'b'** - $\hat{h}(x_4, t)$ and $\hat{u}(x_4, z_1, t)$ are assimilated.

23

Name	Assimil. result	Lines	Related forward solution	Lines	Sensors location:	Bathymetry/ BC at $x = L$	Parameters: $T[s]$, $A[m/s]$, $P[s]$		
E1.1	Fig.6(left) Fig.6(right) Fig.5(right)	1a,2a,3a 1a,2a 2	Fig.5(left)	1,2,3,4	$\hat{h}_1, \hat{u}_1$; $x_1 = 2250m$, y_1 - mid depth	step/open	820	1.0	248
E1.2	Fig.6(left)	1b,2b,3b			as E1.1	step/open	820	1.0	124
E1.3	Fig.6(left)	1c,2c,3c			as E1.1	step/open	820	1.0	62
E2.1	Fig.6(right) Fig.5(right)	1b,2b 4	Fig.5(left)	1,2,3,4	as E1.1	step/open	690	1.0	248
E2.2	Fig.6(right) Fig.5(right)	1c,2c 3	Fig.5(left)	1,2,3,4	as E1.1	step/open	690	1.0	248
E3	Fig.7	1,3,4	Fig.5(left)	1,2,3,4	as E1.1	step/open	690	1.0	248
E4.1	Fig.9(left), Fig.9(right)	1,2 1,2	Fig.8(left) Fig.3	1,2,3,4 $h(x,t)$	$\hat{h}_1, \hat{u}_1$; $x_1 = 3900m$, y_1 - mid depth	pit/open	720	0.5	60
E4.2	Fig.9(left), Fig.9(right)	3 3	Fig.8(left) Fig.3	1,2,3,4 $h(x,t)$	$\hat{h}_1$ as E4.1	pit/open	720	0.5	60
E4.3	Fig.9(left), Fig.9(right)	4 4	Fig.8(left) Fig.3	1,2,3,4 $h(x,t)$	$\hat{u}_1$ as E4.1	pit/open	720	0.5	60
E5.1	Fig.10 Fig.11	1,2 2	Fig.8(right) Fig.4	1,2 $h(x,t)$	$\hat{h}_1, \hat{u}_1$ as E4.1	pit/no-flow	720	0.5	60
E5.2	Fig.10 Fig.11	3 3	Fig.8(right) Fig.4	1 $h(x,t)$	$\hat{h}_1$ as E4.1	pit/no-flow	720	0.5	60
E5.3	Fig.10 Fig.11	4 4	Fig.8(right) Fig.4	2 $h(x,t)$	$\hat{u}_1$ as E4.1	pit/no-flow	720	0.5	60
E5.4	Fig.10	5	Fig.8(right) Fig.4	3 $h(x,t)$	$\hat{h}_1, \hat{u}_2$; $x_1 = 3900m$, $x_2 = 4270m$, y_2 - mid depth	pit/no-flow	720	0.5	60
E5.5	Fig.10	6	Fig.8(right) Fig.4	4 $h(x,t)$	$\hat{h}_1, \hat{h}_2$; $x_1 = 3900m$, $x_2 = 4640m$	pit/no-flow	720	0.5	60
E6.1	Fig.13	1a,2a,3a	Fig.12(left) Fig.3	1,2,3,4	$\hat{u}_1$; $x_1 = 3900m$, y_1 - the bed node	pit/open	3600	0.75	248
E6.2	Fig.13	1b,2b,3b	Fig.12(right) Fig.3	1,2,3	$\hat{h}_1, \hat{u}_1$; $x_1 = 1800m$, y_1 - the surface node	pit/open	3600	0.75	248

Table 1

Summary of numerical experiments

6 Conclusion and discussion

In this paper we present the data assimilation algorithm, which allows assimilation of the velocity and surface elevation measurements into the unsteady flow solution governed by the barotropic fsNSE via open boundary control. We minimize the objective functional using the adjoint sensitivities obtained by solving an inconsistent (discretized continuous) adjoint model described in detail in [16]. In order to derive the adjoint equations we use a mapping in the vertical to shift the problem into a fixed domain; then the variation in the surface variable h is calculated from the Jacobian matrix of the mapping. We should mention that for data assimilation in the ocean and the atmosphere it is commonly accepted using consistent adjoint models obtained by means of automatic differentiation (AD). Because the fsNSE cannot be differentiated in the usual way, the application of AD to the corresponding forward fsNSE solver might not be straightforward. The exact consistent adjoint model could be obtained when applying AD to the TLM solver implementing (15)-(20). Users of models formulated in the surface-terrain following co-ordinates may apply AD directly.

Although both the forward model and the adjoint model developed are non-hydrostatic, open boundaries are hydrostatic, since we build the control invariants based on the characteristics of SWE. We recognize that this approach is approximate. On the other hand, there are practical considerations which may justify it, unless we possess an exact theory of open boundaries for fsNSE (and that looks like a very difficult task). The non-hydrostatic effects are usually associated with the short waves or sharp bed changes (shelf edge). In practice we have some freedom to draw the open boundary. Thus, it has to pass those areas where the bed gradient is moderate. Short waves are not of the main concern in the oceanography anyway. Since the open boundary could be far enough from sensors, the short waves originated from it may have been dissipated due to turbulence or dispersed by short waves of a local origin. Thus, the flow could be controlled from the boundary essentially by long waves. We have seen in Section 5.2 that the non-hydrostatic inconsistency shows itself on the 'error generated' short waves arising in the course of the assimilation. As an example we considered the 'initial shock' in the adjoint solution. We also have demonstrated how the problem of the 'error generated' short waves can be successfully treated by using regularization. Another important consideration is that the control problem is quite robust to the boundary treatment errors. The boundary control of fsNSE by SWE-based characteristic invariants can be regarded as a sort of a weak coupling between the two models. For example, we may consider the output of a global SWE model as a background values for the fsNSE limited area model. Since we do not claim the exact coincidence of the output and input values, the local area model determines the acceptable input values within the control loop. After that the convergence rate usually

noticeably slows down and the iterative process must be stopped. Possibly, even if there are no data to assimilate, non-exact boundary conditions at the open boundary has to be applied in a weak sense. This idea is actually very close to the idea of coupling between the multi-physics domains via 'virtual' control described in [27].

In Section 4 we introduced a regularization method, which has been used in numerical tests described in Section 5. The idea of this method is to extract a certain smooth part of the gradient at each iteration step and use it to build the direction of descent. The key point is how to perform this extraction. We use the CG method working in the Sobolev's space W_2^1 to approximate the gradient starting from its trivial initial value. The advantage of this approach is that it can provide arbitrarily dense family of approximations to the given function (by choosing the order of W_2-space and the parameter α afterwards) compared to the methods based on expansion in a Fourier series, for example. The fact that we process only gradients could be a weak point of this regularization method if working within the CG minimization loop. However, as we have observed in numerous numerical tests, this fits perfectly well with the limited memory LBFGS. A detailed discussion on this subject is beyond the scope of this paper. It is worth noting that this regularization method avoids the practical problem of chosing the regularization parameter. The order of Sobolev's space can be chosen once and then serves well for a wide class of controls. We have found that the parameter α in (36) can be simply taken equal to one.

In Section 5.2 we have considered numerical tests in order to identify a set of incomplete measurements sufficient for solving the open boundary control problem. The main conclusion was that to warrant the solvability we need co-located measurements of the velocity profile and the surface elevation, at least in the sense of the wave-length scale. In reality, the flow is always a mix of progressive and standing waves. Progressive waves can be resolved based on the velocity or the elevation observations collected at any point within the flow (for the 2D cross-sectional model, of course), assimilation results for standing waves depend on the sensor locations. When the set of sensors consists of a co-located pair and a single velocity or elevation sensor, the convergence is apparently dominated by the pair. The additional single sensor, if located in the wave node, may play even a negative part reducing perceptibly the convergence rate. This is an important point that requires us to revise a 'narrow' outlook that more infomation always produces better results from an assimilation.

Acknowledgements

References

[1] T. Ezer, G.L. Mellor, *Simulations of the Atlantic Ocean with a free surface sigma coordinate ocean model*, J. Geophys. Res., 102/15 (1997) 647-657.

[2] V. Casulli, P. Zanolli, *Semi-implicit numerical modelling of non-hydrostatic free-surface flows for environmental problems*, Mathematical and Computer Modelling, 36 (2002) 1131-1149.

[3] M.M. Namin, B. Lin, R.A. Falconer *An implicit numerical algorithm for solving non-hydrostatic free-surface flow problems*, Int. J. Numer. Meth. Fluids 35 (2001) 341-356

[4] J.L. Lions, *Optimal control of systems governed by partial differential equations*, Springer-Verlag, Berlin, New York, 1971

[5] V.A. Solonnikov, *Solvability of the problem of dynamics of viscous incompressible flow bounded by a free surface*, Continuous Media Dynamics, 23 (1975), 123-128

[6] V.I. Sedenko, *Solvability of initial-boundary value problems for the Euler equations of flows on an ideal incompressible non-homogeneous fluid and ideal barotropic fluid that are bounded by free surfaces*, English translation in Russian Acad. Sci. Sb. Math. 83/2 (1995), 347-368

[7] R. Temam, J. Tribbia, *Open boundary conditions for the primitive and Boussinesq equations* J. Atmos. Sci., 60 (2003), 2647-2660

[8] D. Bresch, B.Desjardins, *On viscous shallow-water equations (Saint-Venant model) and the quasi-geostrophic limit*, C.R. Acad. Sci. Paris, Ser. I 335 (2002), 1079-1084

[9] A.V. Fursikov, *Control problems and results on the unique solution of mixed problems by the three-dimensional Navier-Stokes and Euler equations*, Math. Sbornik 115 (1981), 281-306

[10] A. Fursikov, M. Gunzburger, L.Hou *Boundary value problems and optimal boundary control for the Navier-Stokes system: The two-dimensional case*, SIAM J. Cont. Optim. 36, 1998, 852-894

[11] J.L. Lions, *Control of distributed parameters singular systems*, Gauthier-Villars, 1985

[12] H.O. Fattorini, S.S. Sritharan, *Existence of optimal controls for viscous flow problems*, Proc. R. Soc. London A 439 (1992), 81-102

[13] Z. Li, I.M. Navon, M.Y. Hussaini, F.X. Le Dimet *Optimal control of cylinder wakes via suction and blowing*, Computers and Fluids, 32/2 (2003) 149-171

[14] A. Belmiloudi, F. Brossier, *A control method for assimilation of surface data in a linearized Navier-Stokes type problem related to oceanography*, SIAM J. Control Optim., 35 (1997), 2183-2197

[15] A. Belmiloudi *A nonlinear optimal control problem for assimilation of surface data in a Navier-Stokes type equations related to oceanography*, Numer. Funct. Anal. Optim., 39/5 (2001), 1558-1584

[16] I.Yu. Gejadze, G.J.M. Copeland, *Open boundary control problem for Navier-Stokes equations including a free surface: adjoint sensitivity analysis*, Comp. & Math. with Appl., 2005 (under review)

[17] A. Jameson, *Aerodynamic shape optimization using the adjoint method*, Lecture Series at the Von-Karman Institute (2003), Brussels, Belgium

[18] E. Blayo, L.Debreu *Revisiting open boundary conditions from the point of view of characteristic variables*, Ocean Modelling, 9/3 (2005) 231-252

[19] D.C. Liu, J. Nocedal, *On the limited memory BFGS method for large scale minimization*, Math. Prog. 45 (1989) 503-528

[20] J.J. Mor, D.J. Thuente *Line search algorithms with guaranteed sufficient decrease* ACM Transactions on Mathematical Software, 20/3 (1994) 286-307

[21] O.M. Alifanov, E.A. Artyukhin, S.V. Rumyantsev, *Extreme Methods for Solving Ill-Posed Problems with Applications to Inverse Heat Transfer Problems*, Begel House Publishers, 1996

[22] C. Hirt, B. Nichols, N. Romero *SOLA - A numerical solution algorithm for transient fluid flows*, Technical report LA-5852, 1975, Los-Alamos, NM: Los-Alamos National Lab.

[23] A.K. Alekseev, I.M. Navon *The analysis of an ill-posed problem using multi-scale resolution and second order adjoint techniques*, Comput. Methods Appl. Mech. Engrg. 190 (2001) 1937-1953

[24] A.N. Tikhonov, *Solution of incorrectly formulated problems and the regularization method* English translation of Dokl. Akad. Nauk SSSR 151 (1963), 501-504

[25] P. Ch. Hansen, *Rank-deficient and discrete ill-posed problems: numerical aspects of linear inversion* SIAM, 1997

[26] V.A. Morozov *Methods for Solving Incorrectly Posed Problems* Springer, 1984

[27] P. Gervasio, J.L. Lions, A. Quarteroni *Heterogeneous coupling by virtual control methods* Numer. Math., 90 (2001) 241-264